Available online www.jsaer.com

***Journal of Scientific and Engineering Research*, 2019, 6(5):150-159**

Research Article

ISSN: 2394-2630
CODEN(USA): JSERBR

A Hybrid Segmentation Approach of Melanoma based on 2018ISIC-Data Archive

Hamed Abd Ul Aziz, Ahlam Mahmood

Computer Engineering Department, Collage of Engineering, Iraq
hamedce43@gmail.com, ahlam.mahmood@gmail.com

Abstract Early detection of Skin cancer was one of the greatest challenges of dermatologic practice today. Accurate skin lesion segmentation was critical task in all automated system for early diagnosis. This paper presented a triple segmentation procedure based on the pixels distribution Bell-shaped, J-shaped, Reverse J-shaped and U-shaped. According to the nature of dermoscopy images distributions, three segmentation methods were used to identify the normal skin cancer from malignant skin and to extracted the tumor region. First, active contours with selective local or global segmentation were used for bell distribution shape. Second segmentation was done used adjusted ant colony optimization when the U-shaped peaks distribution was classify. Third segmentation strategies applied adaptive threshold for two J-shapes. Experimental results demonstrated the effectiveness of Triple-A method by tested it on 900 dermoscopic images from 2018ISIC data set. The promised accuracies of this method were reach up to 96.87%.

Keywords Segmentation dermoscopy images, ant colony, active contours, adaptive threshold, Histogram

1. Introduction

Early location of malignant skin sore has been consented to be essential because of the wide spread of skin disease just as the financial and fruitful treatment on the off chance that it distinguished early [1]. Dangerous melanomas, the deadliest type of all skin malignant growths, has fix rate of higher than 95% when distinguished at an early stage [2]. Melanoma rate rates have been by and large extending in the latest decades, which makes this one of the harmful developments that has been getting thought both from the general prosperity field, with remedial neutralizing activity fights, and from the sickness ask about field [3].

Today, dermoscopy is a technique used by dermatologists to diagnose skin lesions and thus detect melanomas. Dermoscopy is a strategy that enables specialists to look at structures in the skin that are not noticeable to the exposed eye. At the point when rehearsed by specialists, dermoscopy improves the analytic precision of pigmented skin injuries (PSL) [4-6]. A few strategies have clinicians translate the structures uncovered through dermoscopy.

To gauge and distinguish sets of highlights from dermoscopic images, the mechanized investigation of these images can be amazingly valuable and supportive for dermatologists so as to encourage their conclusion. In view of images gotten by advanced dermoscopy, the points is to build up a helped demonstrative framework for the distinguishing proof of beginning period melanomas. This would enable coordinated course of action of melanocytic wounds. The melanoma location process is made out of the pursue instinctive strides in a standard example acknowledgment handling chain: (a)preprocessing, (b)apply segmentation methodology to isolate the injury zone from the foundation skin, (c)extraction of image highlights for characterization purposes, and (d)and sore arrangement techniques to identification of melanomas and generous in dermoscopy images.

To do a classification of skin lesions must start by confining the sore from solid skin that encompasses each shading image utilizing a segmentation system. The location of this skin sore is a basic issue in dermatoscopic images in light of the fact that the change between the injury and the encompassing skin is hard to identify

precisely. For this, segmentation strategy picked must be exact. This paper, proposed a new pixel distribution-based segmentation, which shares the benefits of the active contour model (ACM), ant colony optimization(ACO) and adaptive thresholding technique(ATT). Using the factual data of the image to apply one of the three models, so it is called triple-A segmentation. The outer part separated to extract melanomas for improves the classification results.

The rest of the paper is sorted out as pursues. Section 2 gives a portrayal of the past work. Section 3 clarify the three image segmentation techniques, the triple-A calculation. Section 4 depicts the trials results and reports on the discoveries. Area 4 gives a dialog, and ends are attracted Section 5.

2. The Theoretical Bases

In the most recent decade, a few frameworks It was suggested to split melanoma. Different methods were produced in Dermoscopy images for border recognition. This non-prominent technique of epidermis imaging has optical amplification and either liquid flooding and low-frequency or cross-energized lighting, making subsurface structures even more visible when compared to traditional clinical imaging.

Late methodologies incorporate thresholding [3,7], k-implies clustering[8], fluffy c-implies clustering [9,10], thickness based grouping [11], mean move clustering [12], angle vector stream snakes [13], shading quantization pursued by spatial segmentation [14], factual district merging [15], watershed transformation [16], and directed learning [17].

In a recent investigation, K. Zhang and others [18], exhibited an area based dynamic shape model (ACM). The advantages of their technique are as per the following: initial another area based marked weight force (SPF) work which can effectively stop the shapes at feeble or obscured edges. Second, the outside and inside limits can be consequently recognized with the underlying form. Third, the ACM with Selective Binary and Gaussian Filtering Regularized Level Set (SBGFRLS) that has the property of specific neighborhood or global segmentation. Fourth, the dimension set capacity can be effectively introduced with a paired capacity, which is more productive to develop than the generally utilized marked separation function (SDF) [18].

Rahil Garnavi et al. proposed automatic segmentation algorithm utilizing shading space examination and bunching dependent on histogram thresholding, it can discover the ideal shading channel [14].

J. Yasmin et al. presents a straightforward yet powerful fringe discovering calculation (improved iterative segmentation calculation utilizing watchful edge locator with iterative separating) for boisterous skin sores, its execution contrasts and that of utilizing shrewd identifier in the outskirt discovery of genuine uproarious skin lesions [19].

So as to naturally isolate the injury from the encompassing ordinary skin, a triple-A segmentation calculation rely upon the measurable circulation of dermatoscopic images, to distinguish the fringe of the sore, has been proposed and talked about in this paper. The proposed calculation comprises of a few stages, which are clarified below.

3. Materials and method

Segmentation is the most important stage for properly dissecting image as it affects the accuracy of the resulting steps. However, due to the incredible verities of the sore shapes, sizes and shades alongside different skin types and surfaces, appropriate segmentation is troublesome. What's more, a few sores have unpredictable limits and now and again there is smooth progress between the sore and the skin. To address this issue, a few calculations have been proposed. They can be extensively named thresholding, edge-based or area based techniques. It consists of several steps, as shown in Figure 1.

3.1. Data pre processing

Dataset is collected from different sources where are 900 images contain both melanoma non melanoma patient information. The source images provided from: "https://challenge2018.isic-archive.com" in size (600x450) pixels. So the first step in the process is resize them to have a fixed width and height (512x512) pixels of all samples. The obtained data set consisted of dermoscopy images with a ground truth segmentation mask annotated by an expert clinician.

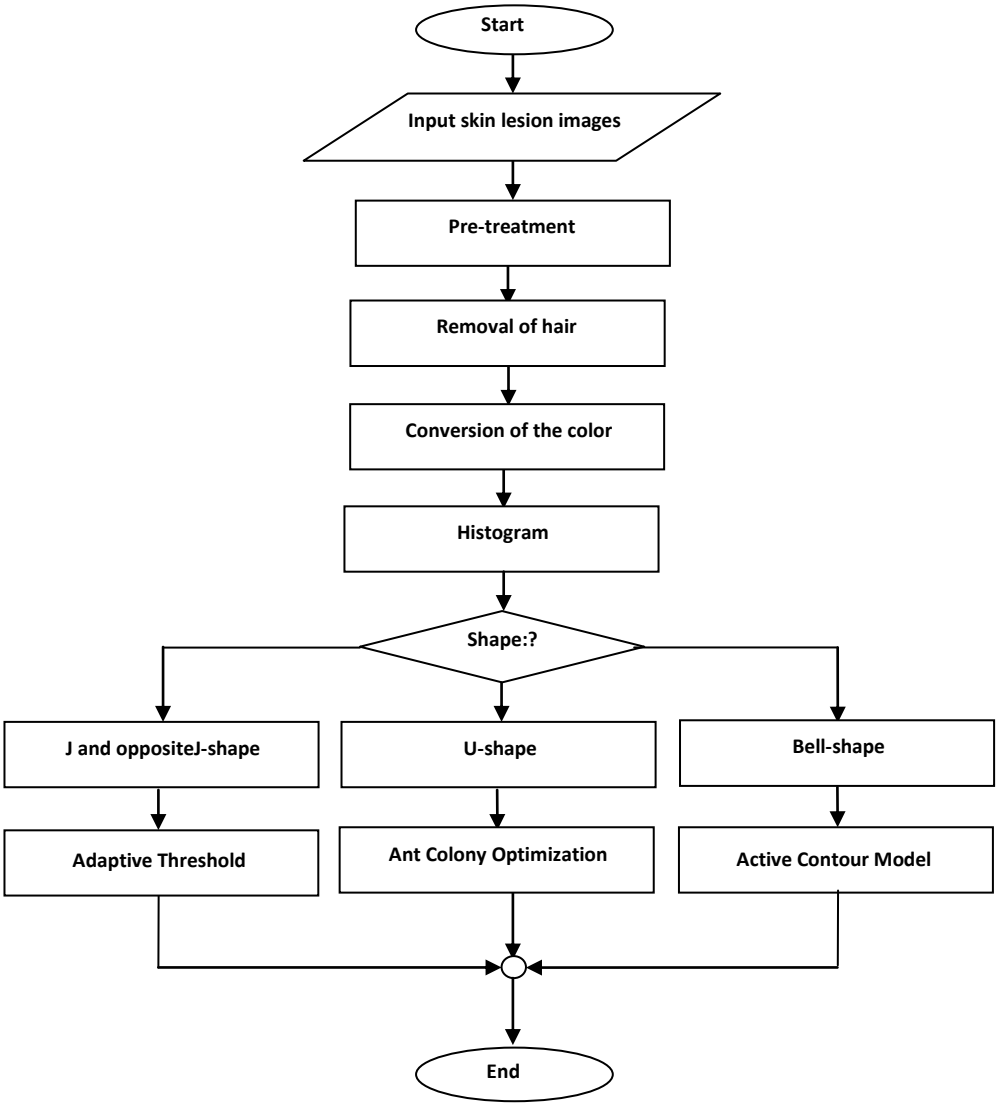

Figure 1: The Proposed Segmentation Process

3.1.1. Hair removal

Injuries blocked with dim thick hairs can cause issues in the segmentation procedure. In such cases, the proposed calculation begins with a hair expulsion preprocessing, which incorporates a grouping of steps. These are: (1) localizing dull hairs, air pockets and names by secluding in cover, (2) using morphological closing operation in vertical, horizontal and diagonal directions, (3) interpolating the expelled hair pixels by close non-hair pixels, and (4)smoothing the last outcome utilizing a median filter to dispense with the staying slim lines.

3.1.2. Color space transformation

Thirdly, to suppress large variations within the background and the lesion, and to reduce the effect of different skin their color variations, the original color RGB images are transformed into intensity (grayscale) ones. The separate values of the three color channels(R, G, B)are combined to produce an intensity image (Y) using a commonly accepted transformation, namely Y=0.3*R+0.59*G+0.11*B[13]. rgb2gray converts RGB values to grayscale values by forming a weighted sum of the R, G, and B components: 0.2989*R+0.5870*G+0.1140 *B.

3.2. Segmentation of tumors depending on allocations of pixels

The motivation behind this progression is independent injury item and foundation into non-covering sets upheld the connected math visual chart that is portrayed the image content and to be that as it may, a reference diagram conveyances are similarly invested to portray entirely unexpected styles of image blessing to express the area technique inside the arranged triple-A standard. regardless of whether determining an importance Visual chart for specific dermoscopic images, it will be recognized as four primary clear shapes, as shown in figure 2 are some broad ones (Gaussian, exponential J, reverse J-shaped and bimodal U-shaped).

For a visual chart association images, if its structured presentation incorporates a profound regular sorrow between 2 crests U-shape. In this way, it's best independent injury from foundation misuse Adjusted hymenopteron Colony improvement (ACO). As its essential property, ACO will in general achieve one best course and if there's very one, it recognizes just 1 of them. Since edges don't appear to be one goals, precisely explains moreover as ants will be positioned on endpoints to accomplish the following likelihood of expelling discontinuity [20]. Hence, this edge location strategy work o.k. when the image gray dimension reference chart is bimodal or almost bimodal. Adaptative Threshold is utilized for J-conveyance or a privilege slanted reference diagram, demonstrating that there have been a larger part of pixels parturition littler qualities. in like manner as visual diagram that is slanted to one side, that have high force pixels. On the contrary hand, a great arrangement of images are commonly on a sporadic premise lit bringing about amultimodal mathematician reference diagram (Figure 2) wherever, in these cases, the standard thresholding procedures perform inadequately or maybe fizzle. amid this classification of, dislike the bimodal case, there's no reasonable partition among article and foundation segment events. In this manner, district based Active Contour Model (ACM) is advantageous to utilized for segmentation. For this visual chart segmentation types beginning, area based marked weight compel perform is utilized, which may speedily stop the forms at frail or obscured edges. Second, the outside and inside limits will be precisely distinguished with the underlying form being wherever inside the image.

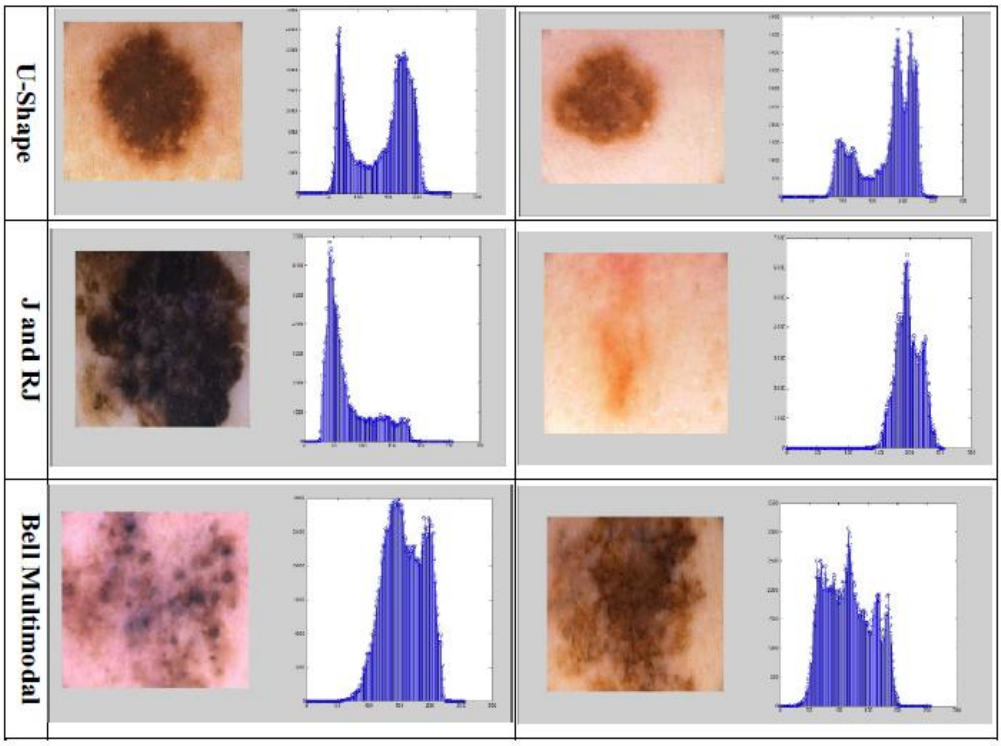

Figure 2: Three Different Dermoscope Quatitative Allocation Images

3.2.1. Adjustedant Colony Optimization (ACO)

ACO has been roused by genuine ants ' scavenging behavior. In ACO, a state of straightforward operators at every age, called unnatural ants, scan for good options. Every artificial ants of an age develops a well-ordered solution. These ants, when fabricate an answer, will assess the fractional arrangement and store some measure of

pheromone on the ground so as to convey between the individuals from their locale which likewise expands the likelihood that different ants will pursue a similar way [20]. ACO comprises of three fundamental parts of starting ants' appropriation, Node progress tenets and pheromone refreshing principle as state in the accompanying sections:-

A. Initialpheromone value and ants' distribution:

Ordinarily beginning pheromone esteems for each conceivable hub are the equivalent however it's conceivable to utilize some essential data to appoint introductory qualities. Angle extent network is an ideal starting pheromone framework because for each pixel it is a basic assessment of the plausibility of becoming nervous.

At first, ants are not haphazardly circulated all over the actual picture, but are isolated into two collections. Initial collection is disseminated by the extent to which image pixels are conceivable borders. Some will be scattered to different image pieces. A few different ants assume the task of perceiving every conceivable pixel of being an edge, irrespective of the fact that it is not accessible on the greatness framework. ACO will generally perform a solitary best course as its essential property and, if there are many, it perceives only one of them. Since edges are not a solitary arrangement, this technique naturally tackles the issue. Equally, starting ant dissemination can be endpoints of a gained edge actual picture.

B. Transition rules:

ACO can be combined effectively of Fuzzy without adjusting its process due to its inclination, particularly supplanting principle. The regular principle that decides next stop for each subterranean ant depends on likelihood esteem registered by Equation 1.

$$P_{i,j}\frac{{\tau_{i,j}}^{\alpha}{\eta_{i,j}}^{\beta}}{\sum_{\epsilon Ni}{\tau_{i,j}}^{\alpha}{\eta_{i,j}}^{\beta}} \quad (1)$$

Where τ_{ij} is pheromone connecting node i to j, η_{ij} is Deterministic data between nodes i and j, α, β Representatives relative impact of pheromone and Deterministic data in choice procedure. A couple of choices are given to register heuristic data, for example, condition 4. In which I is a capacity that gives an estimation of neighbor pixel relations and can be any of conditions 5-8 or comparative ones. x is gray value.

$$\eta_{i,j} = \frac{1}{z}V_c(I_{i,j}) \quad (2)$$

Where $Z = \sum_{i=1:M1}\sum_{j=1:M2} V_c(I_{i,j})$, which is a standardization factor, $I_{i,j}$ is the intensity estimation of the pixel at the position (i,j) of the image I, the function $V_c(I_{i,j})$ is a component of a neighborhood gathering of pixels c (called the clique), and its esteem relies upon the variety of force esteems on the inner clique c (as appeared in Figure 3), the function $V_c(I_{i,j})$ mentioned in [21] is

$$V_c(I_{i,j}) = f(|I_{i-2,j-1} - I_{i+2,j+1}| + |I_{i-2,j+1} - I_{i+2,j-1}| + |I_{i-1,j-2} - I_{i+1,j+2}| + |I_{i-1,j-1} - I_{i+1,j+1}| + |I_{i-1,j} - I_{i+1,j}| + |I_{i-1,j+1} - I_{i+1,j-1}| + |I_{i-1,j+2} - I_{i-1,j-2}| + |I_{i,j-1} - I_{i,j+1}| \quad (3)$$

The last advance on the rule of movement is the passage of ant that happens to one of its past pixels by touching base. Through expanding neighborhood pixels from 8 to 12 (Figure 3), there is an alternative of dynamic neighborhood where ant can escape passing dependent on a half shot once.

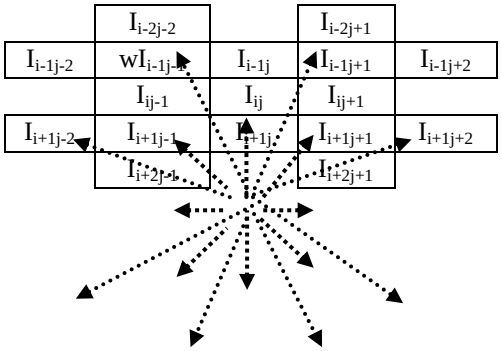

Figure 3: Rising one-time neighborhood to 8 or 12 pixels per ant

C. Pheromone update rule

There are two update forms in every age of ants. At the point when each ant meets its end, as indicated by traits of the way it has gone, pheromone estimation of the voyaged way is refreshed. Likewise when all ants of one age kick the bucket, pheromone is dissipated.

$$\tau_{i,j} = (1-\rho)\tau_{i,j} + \sum_{k=1}^{m} \Delta\tau_{i,j}^{k} \quad (4)$$

In which ρ is pheromone evaporation rate and m is number of ants.

$$\Delta\tau_{i,j}^{k} = \frac{Q}{L_k} \quad (5)$$

Q is a fixed value and L_k is the determined length by k^{th} ant.

D. Decision process

In this move, a boolean determination is taken in every picture element area to specify either it is edge or not by implementing a limit to the last pheromone lattice. The underlying edge T0 is chosen as the average estimation of the pheromone grid. Next, the passages of the pheromone lattice is characterized into two classifications as indicated by the measure that its esteem is less than T0 or bigger than T0. At that point the new limit is figured like the one normal of two average estimations of everyone of them over two classes. The previous procedure is rehashed till the limit esteem It's no longer changing.

3.2.2. Adaptive threshold technique (ATT)

J or reverse J skin image histogram, the segmentation is finished by utilizing a versatile thresholding calculation, which contains three stages: (1) histogram calculation; (2) peak identification; and (3) threshold estimation.

First, the input image is converted into a gray-level image by selecting the channel with the highest entropy [3]. Then, the histogram of intensity, i.e., h(i), i = 0, . . . , 255, is computed constant.

Then extract the most important histogram spikes. If the histogram has a single spike located at i1, the threshold is defined by T=i1+ΔT. The ΔT offset has been empirically tuned and set at 15. If two significant spikes are obtained, the highest possible valley threshold has been chosen. The valley is defined as follows: Two spikes at i1, i2, (i2>i1) define the valley at i as the subtraction result between the pinnacle line and the amplitude of the histogram at i as shown in Figure 4.

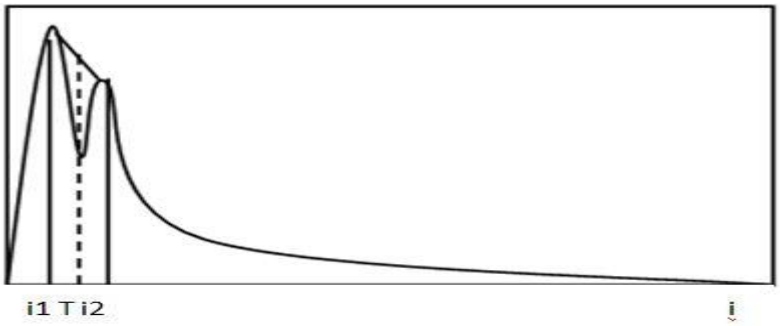

Figure 4: Two spikes Threshold computation

The choice of the most noteworthy peaks in a histogram if multiple pinnacles are recognized includes two stages. To begin with, close pinnacles are blended and supplanted by a solitary pinnacle, i.e., the biggest one. Think about that two pinnacles situated at i1 and i2 are close if |i1 − i2| <δi (Δi = 8). On the off chance that the quantity of pinnacles is bigger than 2 after this progression, the most astounding pinnacle is chosen. At that point, all the staying ones are tried. The 2nd one chosen pinnacle is the one that compares to the biggest profundity of the valley between two histogram spikes.

3.2.3. Active contours model (ACM)

Region-based ACMs have numerous points of interest over edge-based ones. To start with, area based models use the factual data inside and outside the form to control the development, which are less touchy to clamor and have better execution for images with frail edges or without edges. Second, they are essentially less delicate to the area of beginning form and afterward can proficiently identify the outside and inside limits at the same time. A standout amongst the most famous district based models are the C– V and GAC models. Soto section a multimodal ringer histogram which was disperse real picture element on broad variety, break even the upsides of the C– V and GAC models for using the measurable data inside and outside the form to build an area based marked weight force(SPF) function [18]. The fundamental strategies of the suggested calculation are abridged it's like pursues:

1. Introduce the dimension set function ϕ as:

$$\phi(x,t=0)=\begin{cases}-\rho & x\epsilon\Omega_0-\partial\Omega_0\\ 0 & x\epsilon\,\partial\Omega_0\\ +\rho & x\epsilon\Omega_0-\Omega_0\end{cases} \quad (6)$$

where ρ> 0 is a constant, Ω_0 is a subset in the image domain Ω and $\partial\Omega_0$ is the boundary of Ω_0.

2. Compute $c_1(\phi)$ and $c_2(\phi)$, where c_1 and c_2 are two fixed values which are the mean intensities inside and outside the contour for a given image I in domain Ω,

$$c_1(\phi)=\frac{\int_\Omega I(x).H(\phi)dx}{\int_\Omega H(\phi)dx} \quad (7)$$

$$C_2=\frac{\int_\Omega I(x).(1-H(\phi))dx}{\int_\Omega(1-H(\phi))dx} \quad (8)$$

Where H(ϕ) is the Heaviside function

3. Adapt the level set function according to the equation below

$$\frac{\partial\phi}{\partial t}=spf\big(I(x)\big).\alpha|\nabla\phi|,\quad x\in\Omega. \quad (9)$$

$$spf\big(I(x)\big)=\frac{I(x)-\frac{C_1+C_2}{2}}{\max\left(\left|I(x)-\frac{C_1+C_2}{2}\right|\right)},\qquad x\in\Omega. \quad (10)$$

where α constant velocity term a is added to increase the propagation speed and ∇ is the gradient operator.

4. Let ϕ = 1 if ϕ> 0; otherwise, ϕ = -1.

5. Regularize the level set function with a Gaussian filter, i.e. $\phi=\phi*G_\sigma$.

6. Check whether the evolution of the level set function has converged if not, return to step 2.

3. Results and Discussion

In the study, the hybrid segmentation approach is introduced, the dermatoscopic image suspected as melanoma is utilized as info information. To assess the execution of our created framework, this research tests 20 dermatocospic images. The adaptive threshold used in each experiment, by choosing ρ=1, ε=1.5, σ=1, K=5, and time step Δt=1. The α values were set by the images. For various cases, the segmented dermatoscopic image results are shown in Figure 5.

The metrics are used to evaluate the performance of the proposed Triple (AAA) segmentation are: sensitivity (SE), specificity (SP), accuracy (AC) and Computational cost (CC) presented as follows,

$$SE=\frac{Tp}{Tp+FN}*100\% \quad (11)$$

$$SP=\frac{TN}{TN+FP}*100\% \quad (12)$$

$$AC=\frac{Tp+TN}{Tp+FN+TN+FP}*100\% \quad (13)$$

Where TP is the number of true positives, FN the number of false negatives, TN the number of true negative, and FP the number of false positives. The experimental results of total dermatocospy images is described in Table 1.

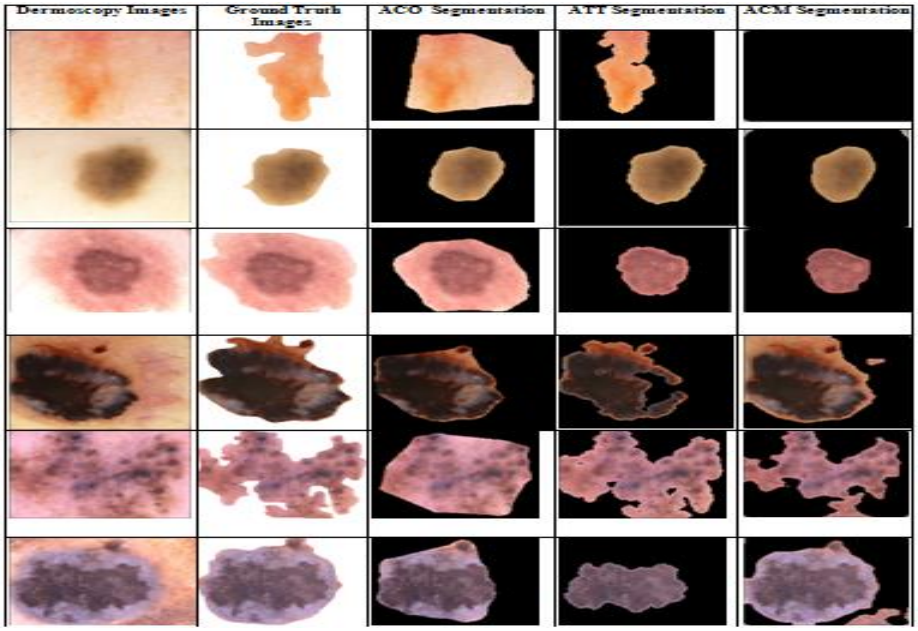

Figure 5: (a) Images of the original skin dermoscopy (b)Ground truth split Images (c) Separated skin areas of split Images utilizing ACO method (d by ATT (e) by ACM.

Table 1: Performance results for the proposed (AAA) system on randomly selected 20 images

Cases	Method	Histogram Classify	SE.	SP.	AC.	CC.
1	Proposed Triple A (AAA) Method	ATT	97.66	97.58	97.60	Low
2		ATT	96.25	94.38	95.17	Low
3		ATT	99.58	97.70	98.17	Low
4		ATT	99.56	95.11	96.63	Low
5		ATT	93.44	99.32	97.28	Low
6		ATT	68.78	99.54	83.32	Low
7		ATT	84.18	99.99	92.75	Low
8		ACO	96.10	96.57	96.35	High
9		ACO	92.82	97.63	95.11	High
10		ACO	96.53	98.82	97.92	High
11		ACO	97.17	97.55	97.35	High
12		ACO	91.26	98.96	95.99	High
13		ACO	90.44	97.53	93.81	High
14		ACO	96.79	91.48	94.08	High
15		ACM	96.43	94.66	95.55	Medium
16		ACM	81.13	99.67	90.10	Medium
17		ACM	85.21	96.45	90.57	Medium
18		ACM	93.31	97.96	95.60	Medium
19		ACM	81.36	99.68	90.10	Medium
20		ACM	97.84	93.08	95.48	Medium

4. Conclusion

This paper has presented an automated approach for lesion segmentation based on the histogram classification. The proposed method is tested on a set of 900 dermoscopy images, this procedure combines advantages of three methods employed are Ant Colony Optimization that's better solution for to U pixels distributions, which ants detect lesions border well. And Adaptive Thresholds Technique if the histogram skewed to the right as well as to the left. Third histogram kinds that's have bell multimodal distribution which possesses the property of local

or global segmentation. Segmentation results are quantitatively assessed by contrasting automated results with manual portioned injuries autonomously drawn by dermatologists. The examination is finished as for four distinct measurements of exactness, affectability, explicitness and computational expense. Trial results show that AAA get the most noteworthy by and large execution contrasted and other computerized strategies referenced in table4 of Ref[22], that have exactnesses from (77.7 to 95.45)%.While AAA improve precision to 96.87% exhibit that the proposed perform well on all images with an alternate injury sorts. Versatile thresholding-based technique, notwithstanding its effortlessness, with an appropriate decision of proposed shading channels is profoundly aggressive with the outstanding skin injury division strategies, and outflanks them with deference to accuracy, particularity, and Acc measurements. Moreover, the proposed ACO is possibly slower since it is endeavor to refresh the pheromone esteems so that the likelihood to produce brilliant arrangements increments after some time.

For the future, the developed procedure hence provides a useful tool as a first stage in the automatic classification melanoma of skin lesion images.

References

[1]. S. Ross-Howe, H.R. Tizhoosh (2018) The Effects of Image Pre- and Post-Processing, Wavelet Decomposition, and Local Binary Patterns on U-Nets for Skin Lesion Segmentation, IEEE World Congress on Computational Intelligence (IEEE WCCI), Rio de Janeiro, Brazil, 8-3.

[2]. J. Abdul Jaleel, S. Salim, Aswin. R.B (2012) Artificial Neural Network Based Detection of Skin Cancer, International Journal of Advanced Research in Electrical, Electronics and Instrumentation Engineering, Volume: 1, 200-205.

[3]. C. Barata, M. Ruela, M. Francisco, et al. (2013) Two Systems for the Detection of Melanomas in Dermoscopy Images Using Texture and Color Features, IEEE Systems Journal, Volume: 12, 1-15.

[4]. M. Zortea, T. R. Schopf, K. Thon, et al. (2014) A Performance of a Dermoscopy-Based Computer Vision System for the Diagnosis of Pigmented Skin Lesions Compared with Visual Evaluation by Experienced Dermatologists, Artificial Intelligence in Medicine, Volume: 60 13–26.

[5]. M. Sadeghi, T. Lee, D. Mclean, et al. (2013) Detection and Analysis of Irregular Streaks in Dermoscopic Images of Skin Lesions, IEEE Transactions On Medical Imaging, Volume: 32, 849 -861.

[6]. N. Smaoui and S. Bessassi 2013 A developed system for melanoma diagnosis, International Journal of Computer Vision and Signal Processing, Volume: 3, 10-17.

[7]. M. E. Celebi, Q. Wen, S. Hwang et al. (2013) Lesion Border Detection in Dermoscopy Images using Ensembles of Thresholding Methods, Skin Research and Technology, Volume: 19 252-258.

[8]. K. Ahmed, T. Jesmin , Z. Rahman (2013) Early Prevention and Detection of Skin Cancer Risk using Data Mining, International Journal of Computer Applications (0975 – 8887) Volume: 62, 1-6.

[9]. L. P. Suresh, K. L. Shunmuganathan , S. H. Krishna (2011) Dermoscopic Image Segmentation using Machine Learning Algorithm", American Journal of Applied Sciences, Volume: 8, 1159-1168.

[10]. H. Lee , Y. P. Chen 2014 Skin cancer extraction with optimum fuzzy thresholding technique, Applied Intelligence, Volume: 40, 415-426.

[11]. A. H. Bhuiyan, I. Azad , K. Uddin (2013) Image Processing for Skin Cancer Features Extraction, International Journal of Scientific & Engineering Research Volume: 4,1-6.

[12]. H. Zhou, G. Schaefer, A. Sadka, et al. (2014) Anisotropic Mean Shift Based Fuzzy C-Means Segmentation of Dermoscopy Images, IEEE Journal of Selected Topics in Signal Processing, Volume: 3, 26-34.

[13]. K. A. Mahmoud , A. Al-Jumaily (2011) Segmentation of Skin Cancer Images Based on Gradient Vector Flow (GVF) Snake, Proceedings of the 2011 IEEE International Conference on Mechatronics and Automation August 7 - 10.

[14]. R. Garnavi, M. Aldeen, M. E. Celebi, et al. (2011) Automatic Segmentation of Dermoscopy Images Using Histogram Thresholding on Optimal Color Channels, World Academy of Science, Engineering and Technology 55, 1040-1048.

[15]. M. E. Celebi, H. A. Kingravi, H. Iyatomi, et al. (2011) Fast and Accurate Border Detection in Dermoscopy Images Using Statistical Region Merging, Medical Imaging 2007: Image Processing, edited by Josien P. W. Pluim, Joseph M. Reinhardt, Proc. of SPIE Volume: 6512, 65123V-1.
[16]. H. Wang, X. Chen, R. H. Moss, et al. (2010) Watershed segmentation of dermoscopy images using a watershed technique, Skin Research and Technology, Volume: 16,1-17.
[17]. M. Elgamal (2013) Automatic Skin Cancer Images Classification, (IJACSA) International Journal of Advanced Computer Science and Applications, Volume: 4, 287- 294.
[18]. K. Zhang, L. Zhang, H. Song, et al. (2010) Active contours with selective local or global segmentation: A new formulation and level set method", Image and Vision Computing, Volume: 28, 668–676.
[19]. J. H. Jaseema Yasmin, M. Mohamed Sadiq (2010) An Improved Iterative Segmentation Algorithm using Canny Edge Detector with Iterative Median Filter for Skin Lesion Border Detection, International Journal of Computer Applications (0975 – 8887) , Volume: 50, 37-42.
[20]. M. Davoodianidaliki, A. Abedin, M. Shankayi (2013) Adaptive Edge Detection using Adjusted Ant Colony Optimization, Remote Sensing and Spatial Information Sciences, Volume: XL-1-W3,123-126 .